A design study for an internal gas-jet target for the heavy-ion storage ring CRYRING

H.T. Schmidt [a], H. Cederquist [a], R. Schuch [a], L. Bagge [b], A. Källberg [b], J. Hilke [b], K.-G. Rensfelt [b], V. Mergel [c], M. Achler [c], R. Dörner [c], L. Spielberger [c], O. Jagutzki [c], H. Schmidt-Böcking [c], J. Ullrich [d], H. Reich [d], M. Unverzagt [d], W. Schmitt [d] and R. Moshammer [d]

[a] *Department of Physics, Atomic Physics, Stockholm University, S-104 05 Stockholm, Sweden*
[b] *The Manne Siegbahn Laboratory, Stockholm University, S-104 05 Stockholm, Sweden*
[c] *Department of Physics, Frankfurt University, D-60486 Frankfurt, Germany*
[d] *Gesellschaft für Schwerionenforschung (GSI), D-64291 Darmstadt, Germany*

This paper presents the design of the internal gas-jet target, CRYJET, which is being constructed for investigations of, e.g., fast ion–atom collisions in the heavy-ion storage and cooler ring CRYRING at the Manne Siegbahn Laboratory, Stockholm University. The goal for the design work was to create an ultra-cold He target ($\leqslant$ 10 mK in the longitudinal direction and 0.5 mK transverse temperature) with a density of $\sim 10^{12}$ atoms/cm^3. Care was taken in order to minimize the influence from the jet on the very low background pressure in the storage ring ($\sim 10^{-11}$ mbar). The low temperature is essential for the resolution in the experiments. The high density will enable us to get sufficient luminosities for investigations of processes with cross sections down to the 10^{-27} cm^2 range. The gas-jet target will be equipped with two recoil-ion-momentum spectrometers in order to extract detailed information about the collision dynamics.

1. Introduction

In the Stockholm heavy-ion storage ring CRYRING a large variety of beams of atomic and molecular ions have been injected, stored, accelerated and electron cooled over the past four years [1]. The qualities of the electron cooled ion beams are excellent in terms of high currents and low emittances. In particular the emittance has been reduced due to the cold adiabatically expanded electron beam used for the electron cooling [2]. The combination of a cold gas-jet target with such ion beams will provide excellent conditions for experiments on fast ion–atom collisions applying the method of recoil-ion-momentum spectroscopy (RIMS) developed at Frankfurt University and GSI [3]. At CRYRING proton beams of MeV energies and $\sim$ 100 μA are available. With this current, a gas target density of 10^{12} cm^{-3}, and a gas-jet diameter of 1 mm we

will have a luminosity of 6×10^{25} cm^{-2} s^{-1}. Therefore, with the expected detection efficiency of 30%, a count rate of one per second is reached for a process with a cross section of 5×10^{-26} cm^2. The possibility to use the gas target to excite stored ions to metastable states and subsequently perform laser- or electron-cooler experiments with the stored metastable ions will also be explored in future experiments.

In this paper we give a description of the gas-jet target, CRYJET, emphasizing in particular the formation of the jet and the influence on the pressure in the ring. In section 2 we give an overall description of the CRYJET stating the technical points, leaving the detailed reasoning behind the various specific technical solutions to sections 3, 4, and 5. In section 3 the acceleration and cooling of a gas flowing with supersonic velocity from a region of high pressure into a vacuum chamber is described in a simple model, and it is demonstrated how the density, flow velocity, and temperature of the gas jet can be calculated under somewhat idealized conditions. The problem of cluster formation at very low source temperatures is also considered in section 3. Section 4 is dedicated to the analysis of heat transport from the warm outer vacuum chamber wall to the cryogenically cooled gas container from which the expanding gas is emerging through a small orifice. In section 5 we estimate the gas load on the storage ring caused by loss of gas from the gas-jet target. A suitable criterion for an acceptable increase in the base-vacuum is that an orbiting ion hits at least ten times more atoms when crossing the gas jet than during the passage of the background gas distributed around the ring of 51.6 m circumference. For a 1 mm diameter jet with a density of 10^{12} atoms/cm^3 this is fulfilled for an average background pressure lower than 10^{-10} mbar. With a 50 l/s high-compression turbomolecular pump on the interaction chamber this corresponds to a maximum acceptable gas load of 5×10^{-9} mbar l/s on the storage ring. In section 5 we discuss the following contributions to the degradation of the storage ring vacuum: backstreaming from the gas-jet dump, the flow of thermalized helium from the jet-formation stages, and finally the scattering of atoms out of the jet due to intra-jet- and jet–background-scattering. As a result of this analysis, we expect a load which is substantially lower than 5×10^{-9} mbar l/s.

2. Technical description of CRYJET

In fig. 1, we show a schematic of the gas-jet target in its position in one of the experimental sections of the storage ring CRYRING. Helium gas at a pressure of $p_0 = 2$ bar is kept in a small container cooled to $T_0 = 30$ K by thermal contact with the cryostage of a *Leybold RGD 1245*. The cryostat is mounted on an (x, y, z)-translational table which is connected to the vacuum chamber with a bellows. This allows for horizontal and vertical displacements of ± 10 mm and 20 mm, respectively. The gas flows through a $\phi = 30$ μm nozzle into a chamber with a vacuum in the 10^{-3} mbar-range maintained by a 500 l/s turbomolecular pump. The gas is accelerated to supersonic velocity (~ 550 m/s) when it flows through the orifice where random thermal energy is transformed into directed kinetic energy. Outside the orifice, the gas expands isentropically leading

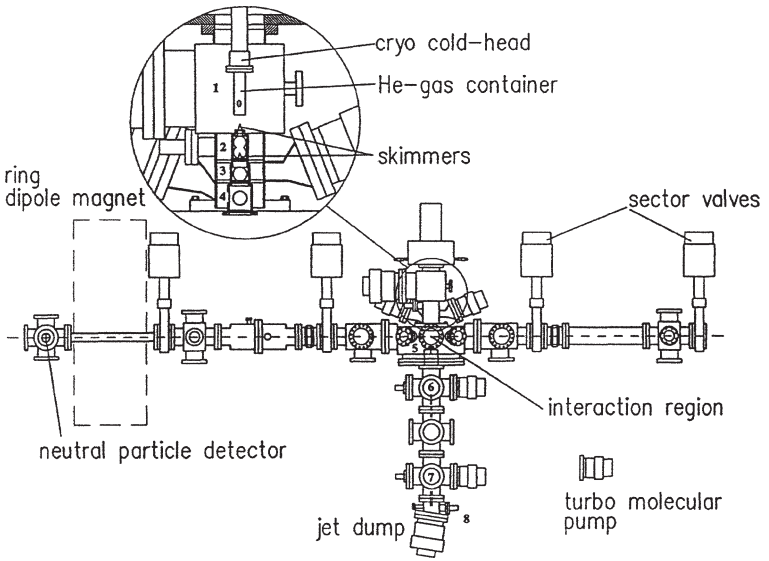

Fig. 1. Schematic of CRYJET installed in one of the straight experimental sections of the CRYRING. The inset shows the jet-formation stages in somewhat more detail. Many of the important parameters are listed in table 1, which refers to the different stages according to their numbers given in the figure.

to cooling to a temperature of $\leqslant 5$ mK. The transversal jet size as well as temperature distribution is then limited by means of a $\phi = 100$ μm skimmer (from *Beam Dynamics Inc*.) at a variable distance of 0–20 mm below the orifice (cf. fig. 1). A second skimmer ($\phi = 300$ μm) is placed 8 cm further downstream and provides the final jet collimation ($\pm 0.15°$). The jet then passes two more differential pump stages, separated by apertures of $\phi = 1$ mm and $\phi = 1.5$ mm through which the jet ideally moves freely. In order to minimize the misalignment of the two skimmers and the two apertures they are mounted together and inserted as one package into the target with helicoflex seals to separate the different vacuum stages (stages 1 to 4 of fig. 1) of the jet-formation system. Finally, the jet is crossed with the stored ion beam in the collision chamber and then it is disposed of in a jet-dump containing three differential pump stages (stages 6 to 8 of fig. 1), which are separated by conductance-limiting tubes. The full jet, under conditions described above, represents a room temperature equivalent gas flow of 3.1×10^{-5} mbar l/s (cf. section 3). In the very unlikely event that the whole jet is lost in the collision chamber there would be an increase in the storage ring background pressure to 6.2×10^{-7} mbar, which is unacceptable. In order to keep the storage ring pressure below 10^{-10} mbar, the fraction of the jet which is lost in the collision chamber due to reflection from the dump or scattering out of the jet from internal collisions or collisions with background gas, has to be smaller than 10^{-4}. In this context it is a very important design criterion that the dump stage acceptance is larger than the collision chamber acceptance as seen from either of the skimmers. This means that atoms scattered into the collision chamber at one of the skimmers are bound to enter the dump.

Table 1
List of CRYJET parameters. The pressures given are *increases* anticipated when neglecting jet–background and intra-jet scattering. The bold numbers refer to the numbered stages of fig. 1.

Hardware:		
Cryostat:		Leybold RGD 1245
Turbomolecular pumps:		
Stage **1** (Expansion chamber)		500 l/s
Stages **2**, **3**, and **4**		200 l/s
Stage **5** (Collision chamber)		50 l/s
Stages **6** and **7**		200 l/s
Stage **8** (Dump)		1 600 l/s
Aperture diameters:		
Nozzle		30 μm
Skimmer 1: (**1**–**2**)		100 μm
Skimmer 2: (**2**–**3**)		300 μm
Orifice 1: (**3**–**4**)		1 mm
Orifice 2: (**4**–**5**)		1.5 mm
Dump-tube (**5**–**6**)	($L = 50$ mm)	5 mm
Dump-tube (**6**–**7**)	($L = 140$ mm)	7 mm
Dump-tube (**7**–**8**)	($L = 90$ mm)	11 mm
Thermodynamic variables:		
Gas container:		
Temperature		30 K
Pressure		2 bar
Gas jet at interaction region:		
Temperatures		$T_{\parallel} \leqslant 5$ mK, $T_{\perp} \approx 0.5$ mK
Density		1.6×10^{12} cm^{-3}
Jet-diameter		1.02 mm
Jet velocity		559 m/s
Gas flow rates:		
Through nozzle		2.6 mbar l/s
Collimated gas jet		3.1×10^{-5} mbar l/s
Background gas from **1**–**4**		6.6×10^{-13} mbar l/s
Background gas from **6**–**8**		8.9×10^{-12} mbar l/s
Vacuum:		
Stage **1**		5.2×10^{-3} mbar
Stage **2**		5.0×10^{-6} mbar
Stage **3**		5.0×10^{-10} mbar
Stage **4**		1.1×10^{-12} mbar
Stage **5**	(CRYRING)	1.9×10^{-13} mbar
Stage **6**		2.0×10^{-12} mbar
Stage **7**		5.0×10^{-10} mbar
Stage **8**		2.6×10^{-8} mbar

The most relevant CRYJET parameters are listed in table 1. The second part of this table ("*Thermodynamic variables*") shows the results of the considerations presented in the following sections. The pressures given for the various stages are estimates of the pressure *increase* when the jet is running. They are obtained under the assumption of perfect alignment of skimmers and apertures, and they do not include effects of collisions involving atoms of the jet. In section 5, we discuss the possible influence of jet–background and intra-jet scattering on the pressures in the ultra-high vacuum stages.

The gas jet has a diameter of ~ 1 mm at the intersection with the ion beam, which occurs at a distance of 284 mm from the first skimmer. The crossing between ion and gas beams is viewed by two recoil-ion momentum spectrometers using electric and magnetic fields to steer recoil ions, and sometimes also free electrons, to position sensitive detectors (micro-channel plates with resistive anodes). For ions and slow electrons the solid angle for detection will be close to 4π. The time-of-flight and position information is used together with the equations for momentum and energy conservation to derive the components of the momentum vectors (for recoil ions and electrons). The fundamental limit for the resolution is given by the gas-jet temperature, which defines the spread in the momenta of the target atoms before the collision. With 5 mK in the longitudinal direction, we get an ultimate momentum spread of 0.02 a.u. (FWHM) in the measurement of the recoil ion momentum along the gas jet direction. The effective transverse temperature will be < 0.5 mK due to the selection of atoms with the lowest transverse velocities by the skimmer system. This will lead to an ultimate momentum spread of 0.006 a.u. (FWHM) in the measurement of the recoil ion momentum perpendicular to the jet. For single-electron capture in 1 MeV proton–He collisions this will lead to an experimental spread in the Q-value of $\Delta Q = 1.0$ eV (FWHM) and a spread in laboratory projectile scattering angle of $\Delta\theta_p = 2$ μrad (FWHM). It is a unique feature of the RIMS technique that this high resolution in general is obtained at the same time as the solid angle is close to 4π.

3. Formation of the gas jet

The ultra-cold supersonic gas jet is formed by letting gas from a high-pressure region pass through a small aperture into a region of low pressure where it expands quasistatically and adiabatically. As the entropy is conserved in the expansion, the decrease in spatial density is accompanied by an increase in momentum-space density or equivalently a decrease in gas temperature. In the following we present a simple but general one-dimensional model, which can account for the temperature drop to the low mK range that takes place in such an expansion. Throughout this section we will apply this model to CRYJET.

The gas is flowing along the positive z-direction from a region of high pressure to one of low pressure (cf. fig. 2). We let $A(z)$ denote the cross section area of the gas jet. The thermodynamic variables p (pressure), n (density), and T (temperature),

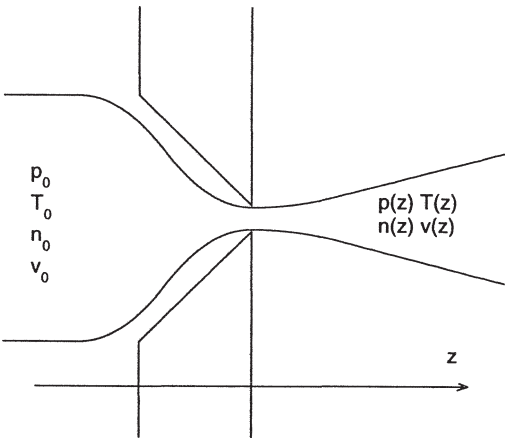

Fig. 2. Schematic of the nozzle and the gas flow through it. $T(z)$, $n(z)$, and $p(z)$ are the temperature, density, and pressure at the distance z from the throat of the nozzle, respectively. $v(z)$ is the flow velocity, i.e. the average velocity in the z-direction. T_0, n_0, p_0, and v_0 are the values of these entities in the cold gas cell. Note that v_0 is small but non-zero.

as well as the flow velocity v are all functions of z and at this point we will assume that they are independent of the transverse coordinates. In the calculation the problem is divided into two parts separately treating the converging and diverging parts. In each of these parts A is a monotonic function of z and we can eliminate z from the problem and give our four unknowns p, n, T, and v as functions of A. That is, for the major part of the discussion to follow, we do not need to know exactly how the jet diverges after the nozzle.

We assume that the gas is ideal and thus that $p = nkT$, where k is Boltzmann's constant. We further assume that the changes in the thermodynamic variables p, n, and T are quasistatic and adiabatic ($\mathrm{d}n/n = (3/5)(\mathrm{d}p/p)$) and that the number of particles are conserved ($\mathrm{d}(nAv) = 0$). The gas is accelerated due to the pressure gradient along z according to Newton's second law: $((\mathrm{d}v/\mathrm{d}t)Mn = -\mathrm{d}p/\mathrm{d}z)$, where M is the mass of a single atom. Applying the ideal gas law, Newton's second law can be written as:

$$\frac{\mathrm{d}p}{p} = -v\frac{M}{kT}\,\mathrm{d}v. \tag{1}$$

Combining the expressions for the conservation of the number of particles and the quasistatic adiabatic process we find:

$$\frac{\mathrm{d}p}{p} = -\frac{5}{3}\left(\frac{\mathrm{d}v}{v} + \frac{\mathrm{d}A}{A}\right). \tag{2}$$

Equations (1) and (2) imply:

$$\left(\left(\frac{v}{s}\right)^2 - 1\right)\frac{\mathrm{d}v}{v} = \frac{\mathrm{d}A}{A}, \tag{3}$$

where s is the local speed of sound:

$$s = \sqrt{\frac{5}{3}\frac{kT}{M}}. \tag{4}$$

If the pressure outside the nozzle, p_1, is only slightly lower than p_0, the pressure gradient, which is the driving force in the acceleration, will be too low to accelerate the gas to the local speed of sound. Hence the flow velocity is always subsonic ($v < s$) and eq. (3) implies that $\mathrm{d}v > 0$ for the converging part ($\mathrm{d}A < 0$) and $\mathrm{d}v < 0$ for the diverging part ($\mathrm{d}A > 0$). If we reduce p_1 we will reach a critical value where the flow velocity reaches the local speed of sound right at the throat (according to ref. [4] this critical value of p_1 is about $0.5\,p_0$). The entity in the parentheses in (3) changes sign at the throat so that $\mathrm{d}v > 0$ also in the diverging part when $p_1 < 0.5\,p_0$. The expansion is now *supersonic* ($v > s$). If p_1 is reduced further we still find that the sound velocity is reached at the throat and we still get the supersonic solution. This is due to the fact that when the flow velocity is higher than the local speed of sound, no information about the changing conditions in the low-pressure region can be transferred backwards through the flowing gas.

Based on the above qualitative arguments, we hence find:

$$v_\mathrm{T} = s_\mathrm{T} = \sqrt{\frac{5}{3}\frac{kT_\mathrm{T}}{M}}, \tag{5}$$

where the subscript T refers to the value at the throat of the nozzle. Using the ideal gas law we see that an alternative expression for a quasistatic adiabatic process is $\mathrm{d}p/p = (5/2)(\mathrm{d}T/T)$. If we combine this with (1) we find:

$$\mathrm{d}T = -\frac{2M}{5k}\,v\,\mathrm{d}v \tag{6}$$

and hence:

$$T_\mathrm{T} - T_0 = -\frac{2M}{5k}\int_{v_0}^{v_\mathrm{T}} v\,\mathrm{d}v \approx -\frac{M}{5k}v_\mathrm{T}^2 = T_\mathrm{T}/3 \quad\Longleftrightarrow\quad T_\mathrm{T} = \frac{3}{4}T_0, \tag{7}$$

where we have used (5) and the fact that $v_0 \ll v_\mathrm{T}$, where v_0 is the average z-component of the velocity in the cold gas cell. With the expressions for the adiabatic quasistatic process, (7) implies that

$$n_\mathrm{T} = \left(\frac{3}{4}\right)^{3/2} n_0 = \frac{3\sqrt{3}}{8}n_0 \tag{8}$$

and

$$p_\mathrm{T} = \left(\frac{3}{4}\right)^{5/2} p_0 = \frac{9\sqrt{3}}{32}p_0. \tag{9}$$

We have now solved the problem for the converging part. This allows us to find the number of particles, N_T, passing the throat per unit time:

$$N_T = v_T n_T A_T = \frac{3}{16} p_0 \sqrt{\frac{15}{kT_0 M}}\, A_T, \tag{10}$$

where A_T is the area at the throat. For our conditions ($p_0 = 2$ bar, $T_0 = 30$ K, and $A_T = \pi(15\ \mu\text{m})^2$) we find $N_T = 6.2 \times 10^{19}$ s^{-1} corresponding to a room temperature equivalent gas leak rate into the expansion chamber (stage 1 of fig. 1) of 2.6 mbar l/s. An expression agreeing with (10) except for a nozzle-shape dependent correction factor of 0.85–1 can be found in ref. [4].

We will now consider the diverging part. By integrating (6) from T_T to T and applying (7) we find that $T = T_0 - (M/5k)v^2$, which in turn implies the following expression for the local speed of sound: $s^2 = s_0^2 - v^2/3$, where s_0 is the speed of sound in the cold gas container. If we introduce $x \equiv v/s_0$ we can write the expression for the temperature as:

$$T = T_0(1 - x^2/3), \tag{11}$$

and (3) can be rewritten as:

$$\int_{A_T}^{A} \frac{\mathrm{d}A}{A} = \int_{x_T}^{x} \left(\frac{x}{1 - x^2/3} - \frac{1}{x} \right) \mathrm{d}x, \tag{12}$$

where $x_T = v_T/s_0 = \sqrt{3}/2$. Solving this integral leads to:

$$\frac{A}{A_T} = \frac{9}{16x(1 - x^2/3)^{3/2}}. \tag{13}$$

From eq. (13) we see that when the gas has expanded to $A/A_T \gg 1$, x becomes close to $\sqrt{3}$ and the flow velocity becomes

$$v_{\text{JET}} = \sqrt{3}\, s_0 = \sqrt{5kT_0/M}, \tag{14}$$

which in our case yields $v_{\text{JET}} = 559$ m/s. It is experimentally established that (14) is correct for monatomic ideal gases [5]. By combining (11) and (13) we find for $A/A_T \gg 1$ that

$$\frac{T}{T_0} = \left(\frac{3\sqrt{3}}{16} \frac{A_T}{A} \right)^{2/3} \tag{15}$$

and hence by the relations for a quasistatic adiabatic process:

$$\frac{n}{n_0} = \frac{3\sqrt{3}}{16} \frac{A_T}{A} \tag{16}$$

and

$$\frac{p}{p_0} = \left(\frac{3\sqrt{3}}{16} \frac{A_T}{A} \right)^{5/3}. \tag{17}$$

Equations (14)–(17) constitute the result of our one-dimensional model calculation.

We assumed in the model that the changes in the thermodynamic variables were quasistatic and adiabatic (i.e. isentropic). We can therefore only expect eqs. (15), (16), and (17) to be valid for a limited range of A, in which $A \gg A_{\mathrm{T}}$ is small enough that a sufficient number of collisions take place to ensure quasistaticity. For larger values of A very few collisions take place and the temperature becomes constant. We hence have a transition from an isentropic to an isothermal expansion. The expression for the density (16) will, however, remain valid even during the isothermal phase, since when there is no further acceleration, n must always decrease inversely proportional to the cross section area.

Since (16) is independent of the transition from isentropic to isothermal expansion, our results for the densities and flows through the system will be much more accurate than the ones for the temperature. We will first determine the density and then return to the problem of the transition from isentropic to isothermal expansion to be able to find an upper limit to the temperature.

In our one-dimensional model we can not find $A(z)$, and we can therefore not use (16) to find the density as a function of z. Instead we will perform a three-dimensional calculation neglecting collisions to establish the density close to the jet-axis as a function of z. We then use (16) to find an expression for $A(z)$ that we can use in (15) and (17) to find the temperature and pressure as a function of z. We formally write the density on axis as:

$$n(0,0,z) = \frac{\eta^{\delta r}(z) N_{\mathrm{T}}}{v_{\mathrm{JET}} \pi \delta r^2}, \tag{18}$$

where δr is the radius of a small disc centered on the z-axis and perpendicular to it. $\eta^{\delta r}(z)$ is the probability for an atom to hit this disc when it is placed at a distance of z from the nozzle. To find $\eta^{\delta r}(z)$ we assume a three-dimensional Maxwell velocity distribution of temperature T_{T} at the throat. We also assume that the transverse velocity component at the throat is conserved. For $z \gg \delta r$ we find:

$$\eta^{\delta r}(z) = \frac{\delta r^2}{z^2} \chi, \tag{19}$$

where χ was obtained by integrating the velocity distribution over the cone in velocity space defined by the acceptance of the disc of radius δr. Using (10), (14), and (19), we can rewrite (18) as:

$$n(0,0,z) = n_0 \frac{3\sqrt{3}}{16} \frac{A_{\mathrm{T}}}{\pi z^2} \chi. \tag{20}$$

We hence identify the density of our one-dimensional model with $n(0,0,z)$. $A(z)$ in the one-dimensional model is thus defined by the opening angle α (half-cone angle) of a homogeneous density distribution with the density given by (20). By combining (16) and (20) we find:

$$A(z) = \pi z^2 (\tan \alpha)^2, \tag{21}$$

where the effective divergence angle, α, is given by $\tan \alpha = \chi^{-1/2} \Leftrightarrow \alpha = 27.1^\circ$. The density at the intersection with the ion beam ($z = 289$ mm) is found from (20)

(or equivalently from a combination of (16) and (21)). We find $n(z = 289\ \text{mm}) = 1.6 \times 10^{12}\ \text{cm}^{-3}$.

The final jet collimation is done by the second skimmer at $z_{\text{sk2}} = 85$ mm with a radius of $r_{\text{sk2}} = 150\ \mu\text{m}$. From (19) and (10) we find the number of atoms passing this skimmer per unit time to be $\eta^{r_{\text{sk2}}}(z_{\text{sk2}})N_{\text{T}} = 7.4 \times 10^{14}\ \text{s}^{-1}$ corresponding to a room temperature equivalent gas jet flow of 3.1×10^{-5} mbar l/s.

In order to be able to extract a prediction for the gas-jet temperature after the cooling, we have to consider the transition from isentropic to isothermal expansion mentioned above. We will assume that the transition is abrupt and that it happens for $A = A_{\text{transition}}$. The final temperature is then found by inserting $A_{\text{transition}}$ in (15).

One criterion for the choice of $A_{\text{transition}}$ could be to take A where the mean free path, $\ell = 1/(\sqrt{2}\, n\sigma)$, where σ is the collision cross section, is equal to 0.01 times the jet-diameter. This limit (Knudsen's number $Kn = 0.01$) is used in the study of gas flow mechanics as the limit of validity of the continuum flow description of quasistatic processes. However, using this criterion here would lead to an unrealistically large value for $A_{\text{transition}}$ and thereby an unrealistically low temperature (few μK). The reason for the failure of this approach is an effect which we could not take into account in our one-dimensional model: We have described the velocity distribution by a single temperature. In reality, however, we have locally after the throat that $T_\perp \ll T_\parallel$, where $T_\perp$ and $T_\parallel$ are the temperature parameters of a two-dimensional Maxwell velocity distribution describing the transverse motion and a one-dimensional distribution describing the longitudinal motion, respectively. The argument for the decrease of the local $T_\perp$, which is strongest in the *absence* of collisions, is a simple geometrical one. Consider, in the absence of collisions, a small volume element inside the gas jet at a distance z from the nozzle. The variation in the transverse velocities of the atoms found in this volume is determined by their transverse positions at the nozzle. If we set the maximal deviation from the average value of the transverse velocity equal to the standard deviation in a two-dimensional Maxwell velocity distribution we find the local transverse temperature in the absence of collisions to be:

$$T_\perp = \frac{M}{\pi k}\,\frac{A_{\text{T}}}{z^2} v_{\text{JET}}^2. \tag{22}$$

For a given $T_\parallel$, the number of collisions taking place in the gas is strongly reduced for $T_\perp \ll T_\parallel$ as compared to $T_\perp = T_\parallel$. $T_\parallel$ will therefore not become as low as it would if we applied the Knudsen number criterion to our one-dimensional model. Toennies et al. [6] assume the cooling to stop when $T_\perp = 0.05\, T_\parallel$. We use this criterion and (22) to determine $A_{\text{transition}}$ and note that (22) is a lower limit to $T_\perp$, since the effect of the collisions is neglected. The corresponding value of $A_{\text{transition}}$ is a lower limit and the temperature given by (15), which we now must identify as the longitudinal temperature, is an upper limit. Using (15), (21), and (22) we find that $T_\perp = 0.05\, T_\parallel$ for $z = 12.0$ mm, and the upper limit for the longitudinal temperature is $T_\parallel = 5$ mK.

The estimate $T_{\parallel} \leqslant 5$ mK was made without using the total scattering cross section for He–He collisions at very low relative velocities. Of course the real final temperature cannot be independent of this. The total scattering cross section for He–He collisions at very low relative velocities is very large. Uang and Stwalley [7] have calculated this cross section to be as high as 1.9×10^{-11} cm^2 for relative velocities of the order of 1 m/s. This very high cross section is related to the existence of a bound state of He_2 [9], and it will act to keep $T_{\perp} = T_{\parallel}$ for the first part of the expansion making $T_{\perp} = 0.05\,T_{\parallel}$ occur for a larger value of z and a lower value of $T_{\parallel}$. We note that the upper limit $T_{\parallel} \leqslant 5$ mK is valid also when internal collisions are taken into account.

Provided that the *local* transverse temperature at the intersection with the ion beam ($z = 289$ mm) is negligible, the *effective* transverse temperature relevant to the experiments will be determined by the acceptance of the second skimmer. An upper limit to the local transverse temperature is found by assuming that the number of collisions is so high that $T_{\perp} = T_{\parallel}$, but in that case the expansion would still be isentropic at $z = 289$ mm and we can use (15) and find $T_{\perp} = T_{\parallel} = 67$ μK. The effective transverse temperature given by the acceptance of the second skimmer ($z_{\mathrm{sk2}} = 85$ mm, $r_{\mathrm{sk2}} = 150$ μm) becomes 0.5 mK, and since this is substantially higher than the upper limit to the local transverse temperature our estimate of the effective transverse temperature will be 0.5 mK.

We will now consider the influence of the background gas in the expansion chamber (stage 1). The total scattering cross section for He–He scattering at velocities of the order of 500 m/s is $\sigma = 4 \times 10^{-15}$ cm^2 [8]. This means that the mean free path of a (helium) atom from the background gas entering the gas jet is much smaller than the diameter of the jet at any position in stage 1. The background gas atoms are therefore not able to enter the jet. As the pressure in the jet according to (17) drops below the background pressure of $p_1 = 5.2 \times 10^{-3}$ mbar (found from (10) and the pumping speed of 500 l/s) within 1 mm after the nozzle, the effect of the background gas atoms on the jet will be to slightly focus the jet. With our standard nozzle–skimmer distance of 5 mm, the change in the jet radius due to this effect is found to be ~ 0.2 mm.

According to [5] the critical parameter for cluster formation with a given nozzle geometry is $\kappa = p_0\sqrt{A_{\mathrm{T}}}/T_0^{4/3}$. For a value of κ corresponding to our conditions and a nozzle with no diverging section, it was found experimentally that $T_{\parallel}$ was increased compared to the value expected without cluster formation [5]. The increase in $T_{\parallel}$ was ascribed to the heat of formation of clusters and that the fraction of atoms which were part of clusters was of the order of 10^{-3} [5]. Since in a jet with a smaller divergence the atoms will spend more time at the density and temperature optimal for cluster formation, a nozzle with a diverging section is expected to make the cluster problem more severe. We will investigate experimentally, whether by decreasing p_0 and using a trumpet shaped nozzle we can keep the target density and reduce the gas load on stage 1 without creating clusters in the jet.

4. Heat transport to the cold gas container

In this section we will estimate the heat flow from the warm part of the target to the cold gas container and conclude that the ~ 12 W cooling power of the Leybold RGD 1245 cryostat is sufficient to keep the cell at 30 K. The gas flow for $T_0 = 30$ K and $p_0 = 2$ bar was given above as 2.6 mbar l/s and cooling from 300 K to 30 K thus requires 0.35 W. The heat conduction through the gas inlet tubes can be reduced to a fraction of 1 W by choosing thin-walled tubes.

The gas container is a copper cylinder of length 85 mm, inner diameter 4 mm, and outer diameter 12 mm. The thick walls are chosen to reduce the temperature gradient along the gas container to less than 1 K. Including a plate for mounting and a 50 mm long section of the gas inlet tube, the cryogenically cooled surface area is approximately $A_c = 40$ cm^2.

With the above mentioned gas load and an effective He pumping speed of 500 l/s we expect a pressure in the expansion chamber of $p_1 = 5.2 \times 10^{-3}$ mbar. The mean free path in the gas is 1.4 cm ($\sigma = 4 \times 10^{-15}$ cm^2 [8]), which is in the transition region between the molecular and continuum flow regions. In the former, heat is transported by atoms carrying energy directly from the warm to the cold surface, whereas the transport in the latter region is limited by atomic scattering. We can thus use the molecular flow result as an upper limit. The power emitted from the outer vacuum chamber walls at temperature T_{chamber} and area A_{chamber} is obtained by averaging the product of the velocity component perpendicular to the surface and the kinetic energy in a Maxwell velocity distribution:

$$P_{\text{EMIT}}^{\text{GAS}} = A_{\text{chamber}} \frac{2}{\sqrt{\pi}} p_1 \sqrt{\frac{2kT_{\text{chamber}}}{M}}. \tag{23}$$

Assuming that the heat absorbed by any surface is simply proportional to the surface area and using the fact that the same amount of heat is absorbed and emitted, we find the heat flow to the cold part by multiplying the power found in (23) by the ratio A_c/A_{chamber}. With our conditions and $T_{\text{chamber}} = 300$ K, we find that this upper limit to the heat flow will be 2.6 W.

The power of the heat *radiated* from the warm surfaces is

$$P_{\text{EMIT}}^{\text{RAD}} = a_{\text{chamber}} A_{\text{chamber}} \sigma_{\text{SB}} T_{\text{chamber}}^4, \tag{24}$$

where σ_{SB} is Stefan–Boltzmann's constant and a_{chamber} is the absorptivity ($\leqslant 1$ per definition). The absorbed power is proportional to the product of the absorptivity and the surface area. In equilibrium we thus find the total power transferred to the cold parts by radiation to be:

$$P_{\text{RAD}} = \frac{a_c A_c}{a_{\text{chamber}} A_{\text{chamber}}} P_{\text{EMIT}}^{\text{RAD}} = a_c A_c \sigma_{\text{SB}} T_{\text{chamber}}^4 = a_c \cdot 1.8 \text{ W} \leqslant 1.8 \text{ W}, \tag{25}$$

where a_c is the absorptivity of the cold surface.

An upper limit for the needed cooling power of the cryostat is thus ~ 5 W, which is well below the 12 W provided by the cryostat. The cold finger is equipped with heating

wires and a temperature gauge, which makes it possible to regulate the temperature to the desired value.

5. The influence of the gas-jet target on the CRYRING vacuum

In this section we estimate the leak rate into the storage ring caused by the gas-jet target. We first want to emphasize that the high-compression turbo pumps of stages 4, 5, and 6, with ultimate pressures of 10^{-11} mbar are essential to keep the vacuum conditions even without running the jet. We have tested a high-compression turbo pump and observed a pressure in a UHV-test chamber in the low 10^{-11} mbar-range.

The main contribution to the leak rate of the running jet will be backstreaming gas from the gas-jet dump, but also leaks from the jet formation system will contribute. Furthermore we have to consider the effect on the vacuum by atoms scattered out of the jet either by background gas atoms or by other jet atoms. The maximum acceptable total gas load on the ring is 5×10^{-9} mbar l/s corresponding to the loss of approximately 1 out of 10^4 atoms of the jet.

The jet passes through the dump stages directly into a 1600 l/s turbomolecular pump (1200 l/s He pumping speed at 10^{-8} mbar), which is placed off-center and tilted in order to minimize the interaction between the gas-jet and the first rotor of the pump. This should increase the effective pumping speed by a factor of two, but to be conservative we will assume an effective pumping speed of 1200 l/s in the following. Using the gas load of the jet found in section 3 (3.1×10^{-5} mbar l/s), we expect the pressure in the last dump stage (stage 8) to be $p_8 = 2.6 \times 10^{-8}$ mbar.

A schematic of the dump is shown in fig. 3. ϕ_{i-j} denotes the flow from stage i to stage j and C_{i-j} is the conductance between these stages. S_i is the pumping speed in stage i. The pressure p_8 is constant and the aim in the design is to minimize the flow into the storage ring $\phi_{6\text{–}5}$ for a given gas jet flow. The conductance of a tube is reduced by a factor close to the ratio of the diameter to the length of the tube (the exact reduction factors are tabulated in ref. [4]) in comparison to a simple orifice of the same area A ($C = \sqrt{kT/(2\pi M)}\, A$). If we neglect $\phi_{7\text{–}6}$ we find:

$$p_7 = p_8(1 + S_7/C_{8\text{–}7})^{-1}. \tag{26}$$

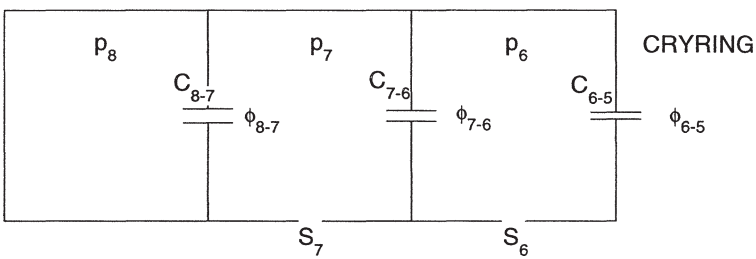

Fig. 3. Schematic view of the gas-jet dump with the three differential pump stages.

This equals 5.0×10^{-10} mbar with $S_7 = 200$ l/s and $C_{8\text{–}7} = 3.9$ l/s.

We must add to the flows $\phi_{7\text{–}6}$ and $\phi_{6\text{–}5}$ "direct" flows from the parts further down in the dump. For small angles, Θ, from the direction straight through all the dump sections the flux of gas from a tube will be the same as for an orifice, which in turn is well described by a $\cos\Theta$-distribution. In a $\cos\Theta$-distribution the forward flux (i.e. $\Theta \approx 0$) is twice that of an isotropic distribution. We have then for the direct contribution to $\phi_{7\text{–}6}$:

$$\phi_{7\text{–}6}^{\text{direct}} \approx 2p_8 C'_{8\text{–}7} \frac{\pi r_{7\text{–}6}^2}{d_7^2} = p_8 C'_{8\text{–}7} \frac{r_{7\text{–}6}^2}{d_7^2}, \tag{27}$$

where $r_{7\text{–}6}$ is the radius of the tube separating stages 7 and 6, $d_7 = 45$ cm is the distance between this tube and the one separating stages 8 and 7 and $C'_{8\text{–}7}$ is the conductance of a simple orifice with the same diameter as the first tube. We can now find the pressure of the dump-chamber closest to CRYRING, p_6:

$$p_6 = p_7(1 + S_6/C_{7\text{–}6})^{-1} + \phi_{7\text{–}6}^{\text{direct}}/S_6. \tag{28}$$

For p_6 the direct contribution is only 13% of the total value $p_6 = 2.0 \times 10^{-12}$ mbar. The flow into CRYRING will have contributions from all three chambers:

$$\phi_{6\text{–}5} = p_6 C_{6\text{–}5} + p_7 C'_{7\text{–}6} \frac{r_{6\text{–}5}^2}{d_6^2} + p_8 C'_{8\text{–}7} \frac{r_{6\text{–}5}^2}{(d_7 + L_{7\text{–}6} + d_6)^2}, \tag{29}$$

where $r_{6\text{–}5}$ is the radius of the tube closest to CRYRING, $L_{7\text{–}6}$ is the length of the middle dump tube and $d_6 = 25$ cm is the distance between the two dump tubes connected to stage 6. We find the result: $\phi_{6\text{–}5} = 8.9 \times 10^{-12}$ mbar l/s implying a pressure increase in the collision chamber of 1.8×10^{-13} mbar. 78% of the flow is the direct flow from the first tube represented by the last term of (29). The optimal tube configuration was found by a numerical optimization procedure. $\phi_{6\text{–}5}$ was minimized by varying the diameters and lengths of, as well as the distances between, the dump tubes. This was done with the restriction that sufficient space was given for the jet to pass through these elements into the dump allowing for small mechanical errors.

When evaluating the flow of thermalized helium from the jet-formation system the first thing to notice is that there will be no "direct flow" contribution from the stages 1 and 2 since the collimation performed by the (remaining part of) the jet formation system will make such a direct flow enter the gas-jet dump. As mentioned in section 2 this also means that atoms scattered into the collision chamber by one of the skimmer edges are bound to enter the dump. We will treat this problem analogous to the dump problem as a three-stage problem starting from a fixed pressure of stage 2. To find the pressure in stage 2 we must evaluate the by far dominating contribution to the flow into this chamber, namely the fraction of the gas jet which passes the first skimmer but not the second one. In section 3 we found the total flow from the nozzle and the probability of passing the second skimmer. We can of course in an analogous way find the probability of passing the first skimmer for a nozzle–skimmer distance of 5 mm and thereby the total flow into stage 2. With a pumping speed of $S_2 = 200$ l/s

we find that the pressure of stage 2 will be $p_2 = 5.0 \times 10^{-6}$ mbar. From here the problem is identical to the dump problem except that we shall not include a direct flow from stage 2 into the collision chamber. We find the pressures and flows stated in table 1. The total flow of thermalized helium from the jet-formation stages is found to be 6.6×10^{-13} mbar l/s.

If we neglect the possible influence of jet–background and intra-jet scattering to be discussed below, the gas-jet target represents a total CRYRING leak of 9.6×10^{-12} mbar l/s. With a 50 l/s pumping speed at the collision chamber this leads to a pressure rise in this region of only 1.9×10^{-13} mbar.

We now consider the contribution to the background pressure in the collision chamber from scattering of atoms out of the jet. This can be caused either by collisions between jet and background gas atoms or between atoms of the jet. Due to the collimation effect of the jet-formation system we can have no contributions from the stages 1 and 2. For the jet–background collisions we know the total cross section $\sigma = 4 \times 10^{-15}$ cm^2 [8]. Under the extremely pessimistic assumption that all jet–background scattering events in stage 3 would fall in the small interval of scattering angles causing the scattered jet atom to enter the collision chamber but miss the dump, this effect would lead to an increase of the collision chamber pressure of 2.6×10^{-13} mbar. It therefore seems as if we can neglect the jet–background collisions in this context.

Due to the high velocity in the forward direction only those intra-jet scattering events leading to transverse velocities higher than 5 m/s can contribute in a single collision to raising the background pressure in the collision chamber. To get this high transverse velocity the difference in longitudinal velocity of the two colliding atoms must be higher than 10 m/s at the same time as the scattering angle must be close to 90°. With a maximum longitudinal temperature of $T_{\|} = 5$ mK the standard deviation of the longitudinal velocity will be 3.2 m/s making the above scenario highly unlikely. On the other hand, due to the extremely large cross section for scattering at low relative velocities [7] an atom with a longitudinal velocity deviating by 3.2 m/s from the average will make about 1–5 collisions on the way through the interaction region. These will probably mostly be small angle scatterings but will nevertheless contribute to making the sharp border of the jet defined by the skimmers less sharp, and hence allow for a tail in the spatial distribution to build up. Without knowledge of the differential cross section at velocities in the few m/s range, we can not estimate whether this effect will contribute to loss of jet atoms to the background gas, but should it cause serious vacuum problems the low backflow from the jet dump indicates that the diameter of the dump-entrance tube can be made somewhat larger.

6. Conclusion

The main conclusion from our design study is that we can obtain a target with a density of about 10^{12} cm^{-3} and longitudinal and transverse temperatures of $\leqslant 5$ mK

and ~ 0.5 mK, respectively. For the RIMS experiments to be performed, the transverse temperature, which is determined by the geometry, will usually be the most important one. A low $T_{\|}$ is, however, important in order to minimize the effects of intra-jet scattering, in particular $T_{\|} \leqslant 5$ mK means that intra-jet single scattering events resulting in jet atoms leaving the acceptance of the dump become highly unlikely. Our estimates of the pressures in the various stages of the target indicate that the high density can be obtained at the same time as the ultra-high vacuum conditions of the storage ring are maintained.

For the real gas-jet target to meet the ambitious design values presented here, we consider two technical aspects to be of crucial importance: The compactness of the system, and the use of high-compression turbomolecular pumps for the stages with the lowest pressures. The short flight distances leave little time for internal collisions to change the square transverse velocity distribution defined by the skimmers into a Maxwellian distribution with Gaussian tails causing atoms to miss the dump. It is also crucial that the skimmer configuration is such that scattering at one of the skimmers can not contribute to an increase in the collision chamber pressure. Furthermore the compactness makes it feasible to maintain ultra-high vacuum conditions with high-compression turbomolecular pumps with moderate pumping speeds.

Acknowledgements

The gas-jet target project is financed by the Knut and Alice Wallenberg Foundation and the Swedish Natural Science Research Council. One of the authors (HTS) wishes to thank the Danish Natural Science Research Council for financial support.

References

[1] K. Abrahamsson et al., Nucl. Instr. Methods B 79 (1993) 269.
[2] H. Danared, Nucl. Instr. Methods A 335 (1993) 397;
H. Danared et al., Phys. Rev. Lett. 72 (1994) 3775.
[3] R. Dörner et al., Nucl. Instr. Methods B 99 (1995) 111;
V. Mergel et al., Phys. Rev. Lett. 74 (1995) 2200;
L. Spielberger et al., Phys. Rev. Lett. 74 (1995) 4615;
R. Moshammer et al., Phys. Rev. Lett. 77 (1996) 1242.
[4] J.F. O'Hanlon, in: *A User's Guide to Vacuum Technology* (Wiley, New York, 1989) p. 29.
[5] H. Buchenau, E.L. Knuth, J. Northby, J.P. Toennies and C. Winkler, J. Chem. Phys. 92 (1990) 6875.
[6] J.P. Toennies and K. Winkelmann, J. Chem. Phys. 66 (1977) 3965.
[7] Y.-H. Uang and W.C. Stwalley, J. Chem. Phys. 76 (1982) 5069.
[8] M.G. Dondi, G. Scoles, F. Torello and H. Pauly, J. Chem. Phys. 51 (1969) 392.
[9] F. Luo, G.C. McBane, G. Kim, C.F. Giese and W.R. Gentry, J. Chem. Phys. 98 (1993) 3564.